J Mater Sci: Mater Med (2007) 18:1287–1298
DOI 10.1007/s10856-006-0062-5

# Titanium dioxide ($TiO_2$) nanoparticles filled poly(D,L lactid acid) (PDLLA) matrix composites for bone tissue engineering

**L.-C. Gerhardt · G. M. R. Jell · A. R. Boccaccini**

Received: 23 December 2005 / Accepted: 13 March 2006 / Published online: 9 January 2007


**Abstract** Titanium dioxide ($TiO_2$) nanoparticles were investigated for bone tissue engineering applications with regard to bioactivity and particle cytotoxicity. Composite films on the basis of poly(D,L lactid acid) (PDLLA) filled with 0, 5 and 30 wt% $TiO_2$ nanoparticles were processed by solvent casting. Bioactivity, characterised by formation of hydroxyapatite (HA) on the materials surface, was investigated for both the free $TiO_2$ nanoparticles and PDLLA/$TiO_2$ composite films upon immersion in supersaturated simulated body fluid (1.5 SBF) for up to 3 weeks. Non-stoichiometric HA nanocrystals (ns-HA) with an average diameter of 40 nm were formed on the high content (30 wt% $TiO_2$) composite films after 2 weeks of immersion in 1.5 SBF. For the pure PDLLA film and the low content composite films (5 wt% $TiO_2$) trace amounts of ns-HA nanocrystals were apparent after 3 weeks. The $TiO_2$ nanopowder alone showed no bioactivity. The effect of $TiO_2$ nanoparticles (0.5–10,000 μg/mL) on MG-63 osteoblast-like cell metabolic activity was assessed by the MTT assay. $TiO_2$ particle concentrations of up to 100 μg/mL had no significant effect on MG-63 cell viability.

L.-C. Gerhardt · G. M. R. Jell · A. R. Boccaccini (✉)
Department of Materials, Imperial College London, Prince Consort Road, London SW7 2BP, UK
e-mail: a.boccaccini@imperial.ac.uk

L.-C. Gerhardt
Lehrstuhl für Medizintechnik, TU Munich, Boltzmannstrasse 11, 85748 Garching bei Munchen, Germany

*Present Address:*
L.-C. Gerhardt
Laboratory for Protection and Physiology, EMPA, Materials Science and Technology, 9014 St. Gallen, Switzerland

## 1 Introduction

Scaffolds for bone tissue-engineering and bone analogue materials should be processed to mimic the biological and mechanical properties of bone [1]. Composites made of biodegradable polymers containing bioinert or bioactive ceramic phases attract increasing interest because the mixed material composition can exhibit favourable mechanical properties and can eliminate elastic modulus mismatch and stress shielding effects when used as bone replacement material or as scaffold for bone regeneration [2–5]. Biomimetics, i.e., mimicking the structure and surface of living tissues in artificial materials, is considered a promising method for designing improved biomaterials by helping to prevent fibrous encapsulation and promoting osseointegration [6]. Insufficient bond to bone tissue is considered a major cause of aseptic implant failure and it is often associated with implant deterioration and generation of wear particles [7, 8]. Particulate wear induces a local inflammatory response that leads to periprosthetic osteolysis and aseptic implant loosening [9–11].

Hydroxyapatite (HA), alumina or $TiO_2$ nanocrystals (i.e., crystals with grain sizes <100 nm [12]) possess the ability to simulate the nanometre surface topography and roughness found in osseous tissue [13–15]. In several investigations, ceramic nanoparticles used in bone replacement materials have been shown to

influence positively the cellular behaviour compared to conventional particles in micrometer dimensions [13–20]. Thus, ceramic nanoparticles may have greater efficacy for bone tissue engineering applications, than micro-sized particles, e.g., $TiO_2$ nanoparticles are being considered in implant or scaffold design strategies to induce differences in cellular behaviour [16–20]. $TiO_2$ nanoparticles may affect the cellular behaviour differently to micro-sized particles and these properties may be utilized to improve osseointegration.

In this study, PDLLA-based composite films filled with different $TiO_2$ nanoparticles concentrations (5, 30 wt%) were exposed to supersaturated simulated body fluid (1.5 SBF) to assess bioactivity, i.e., to examine the ability of the polymer-ceramic composites to nucleate and deposit HA crystals on the materials surface in vitro. This process is known in literature as the ''biomimetic process'' [6, 21–24]. Since preliminary experiments in our laboratory have shown no evidence of bioactivity by soaking the composites in standard SBF [25], a tailored, modified simulated body fluid with ion concentrations 1.5 times those of SBF was used.

Bone tissue engineering scaffolds and bone prostheses designed with ceramic nanoparticles ($TiO_2$, $Al_2O_3$, HA) may release wear debris nanoparticles. Subsequently, bone cells would come into direct contact with the particles leading to nanoparticle-cell interactions. For this reason, the cytotoxic effects of $TiO_2$ nanoparticles on cellular functions of osteoblast-like MG-63 cells were investigated.

## 2 Experimental

### 2.1 Materials

Polymer granules of amorphous poly(D,L lactid acid) (PDLLA) with an inherent viscosity of 1.62 dL/g were obtained from Purac (Purasorb PDL, Purac biochem, Gorinchem, The Netherlands) and used to produce the film matrix.

As filler material for the composite films as well as particles for the cell culture experiment, commercially available $TiO_2$ nanopowder (Aeroxide® P25, Degussa, Frankfurt a. M., Germany) with an average size of 21 nm and a specific surface area of 50 $m^2/g$ was employed. Crystallographically, the nanoparticles consist of approximately 80% anatase and 20% rutile [26].

### 2.2 Sample preparation

A polymer stock suspension was prepared in three separated centrifuge tubes. The PDLLA pellets were dissolved in dimethyl carbonate (DMC, Sigma-Aldrich, Steinheim, Germany) to produce an initial polymer weight to solvent ratio of 5% (w/v) by interspersing 600 mg of PDLLA in 12.0 mL of DMC. The polymer stock suspension was then magnetically stirred for at least 12 h to obtain a homogeneous polymer solution. For the composites, $TiO_2$ nanoparticles were added to a final concentration of 5 and 30 wt% with respect to the polymer.

Subsequently, the mixture was sonicated for 30 min at 250 W (Ultrawave JP200, Ultrawave, Cardiff, UK) to improve the dispersion of $TiO_2$ particles in the polymer solution and to destroy possible titanium dioxide agglomerations. Glass slides (Microscope Glass Slides, BDH, Dorset, UK) were pre-treated with sugar acid etchant for improved adhesion of the PDLLA-based films to avoid peeling off effects during film immersion in 1.5 SBF.

Prior to solvent casting, the glass slides used as substrate for the films were degreased and washed by soaking in HCl (1N), acetone and finally DMC. Then, an aliquot (1 mL) of the polymer-ceramic solution was cast and spread onto the glass slides (76 mm × 26 mm) using a pipette.

The slides were carefully covered with Petri dishes for 24 h to ensure slow DMC solvent evaporation. Altogether, three different series of PDLLA films containing 0, 5 or 30 wt% $TiO_2$ nanoparticles were fabricated and exposed to 1.5 SBF. The nominal thickness of the films was in the range 10–15 μm.

### 2.3 Immersion procedure in 1.5 mM simulated body fluid (1.5 SBF)

In vitro bioactivity studies were carried out using supersaturated SBF (1.5 SBF). 1.5 SBF was prepared on the basic formulation of conventional SBF [27], which contains ion concentrations nearly equal to those of human blood plasma. Supersaturated SBF was prepared by dissolving respective amounts of NaCl, $NaHCO_3$, KCl, $K_2HPO_4{\cdot}3H_2O$, $MgCl_2{\cdot}6H_2O$, $CaCl_2{\cdot}2H_2O$, and $Na_2SO_4$ (Sigma-Aldrich, Steinheim, Germany) into ultra-pure water (Ultrapure water system, Nanopure Diamond, Barnstead Thermolyne, Dubuque, USA). The 1.5 SBF solution was buffered by 75 mM tris(hydroxyl-methyl) aminomethane and adjusted at 37 °C to a physiological pH 7.25 by approximately 67.5 mM hydrochloric acid (HCl) [27].

After solvent evaporation overnight, the films were carefully rinsed with 70% ethanol and twice with ultrapure water. Then, each film attached to the glass slides was vertically positioned in a separate centrifuge tube, and subsequently 35 mL of supersaturated SBF

(37 °C) was added. The ratio of film mass to SBF solution volume was ~0.7 g/L. The films were then transferred to an orbital shaker (C24 Incubator Shaker, New Brunswick Scientific, Edison, USA), which rotated at 175 rpm at a controlled temperature of 37 °C. The SBF was refreshed every 5 days after the start of the experiment. The films were collected after 4, 7, 14 and 21 days of incubation, followed by rinsing in ultrapure water. The samples were then stored in a desiccator prior to analysis.

For the assessment of the bioactive characteristics of the particles themselves, an amount of 100 mg of $TiO_2$ powder was placed in a centrifuge tube. Then, 30 mL of 1.5 SBF was added. The nanoparticle-SBF mixture was incubated for 3 weeks using the orbital shaker that maintained a constant temperature of 37 °C and rotated at 175 rpm. At the point of extracting the powder from supersaturated SBF, a thin spoon was used and the wet powder was placed in a glass Petri dish. The powder was gently rinsed using acetone with subsequent solvent evaporation overnight under a fume hood.

### 2.4 Composite film characterisation

All the films were inspected with a field emission gun scanning electron microscope (FEG-SEM LEO 1525, Carl Zeiss SMT, Cambridgeshire, UK) to obtain high-resolution low voltage surface images with minimal damage to the polymer. Surface morphology, film homogeneity and uniformity of the dispersion of $TiO_2$ nanoparticles in the PDLLA matrix as well as possible particle agglomeration within the composites were qualitatively characterised. Small pieces of the films were mounted on metallic stubs using double-sided adhesive carbon tapes and sputtered for 2 min with gold. Accelerating voltages in the range of 5–15 kV were used for the examination of microstructures on cross-sections and to observe surface topography. Secondary electron images (SEI) were usually taken since the topography of the composite films was of major interest.

To quantitatively characterise the surface topography of the as-prepared composite films, scanning white light interferometry was carried out using a Zygo™ metrology system (NewView 200, Zygo, Middlefield, CT, USA) equipped with the MetroPro™ software.

As-prepared and degraded films after immersion in 1.5 SBF were also characterised by Raman spectroscopy (RM 2000, Renishaw, Gloucestershire, UK) connected to a Leica microscope (objective magnification × 20, NA = 0.4). The samples were illuminated with a 785 nm diode laser (~300 mW) and the subsequent spectra were recorded for 20 s in the wavenumber interval of 250–1900 $cm^{-1}$. Five different locations within a sample area of approximately 1 $cm^2$ were examined for each film since non-homogeneous formation of HA on their surfaces was expected. Three spectra per location were recorded.

Selected films were analysed using a powder diffraction system (Philips PW1710, Eindhoven, The Netherlands), in order to confirm the crystallinity of possible HA formation. The films were exposed to high energetic (Cu–K$\alpha$, $\lambda$ = 1.5406 Å) X-rays and the $2\theta$ angles were recorded using a scintillation counter in the $2\theta$ interval between 5° and 65° at scan steps sizes of 0.04° and a detection time of 1.5 s per scan.

### 2.5 Cells and culture conditions

The human bone-like osteosarcoma cell line MG-63 was obtained from the European Collection of Cell Cultures (ECCAC, Salisbury, UK). All cell culture reagents were purchased from Gibco, Paisley, UK, if not otherwise stated. The cells were cultured in Dulbecco's Modified Eagles Medium (DMEM) supplemented with 10% foetal bovine serum, 1% non-essential amino acids, 1% L-glutamine (0.2 M) and 1% of antibiotic and antimycotic (10,000 Units/mL penicillin, 10 mg/mL streptomycin and 25 μg/mL amphotericin B). The osteoblast-like cells were incubated at 37 °C and 5% $CO_2$. Prior to the experiments, MG-63 cells were trypsinised using trypsin/EDTA for 5 min, centrifuged at $200 \times g$ for 5 min, and resuspended in the medium.

### 2.6 Particle preparation, cell seeding and treatment of cells with $TiO_2$

Titanium dioxide nanoparticles were sterilised by prolonged (4 cycles) steam treatment in an autoclave at 134 °C and 2.05 bar. Prior to a final nanoparticle dilution, a 10 mg/mL stock solution (mixture of 100 mg $TiO_2$ in 10 mL DMEM) was sonicated in an ultrasonic bath (Ultrawave JP200, Ultrawave, Cardiff, UK) for 20 min at 250 W and vortexed (Clifton Cyclone Vortex Mixer CM-1, Nickel-Electro, North Somerset, UK) for 30 s at full power in order to disseminate possible $TiO_2$ particle agglomerations.

Cells were seeded at a concentration of 10,000 cells/well in a 96-well plate. After a 24 h incubation period the cells were observed under an inverse phase microscope to assess cell morphology. Cell culture medium was then aspirated and 0.2 mL of fresh medium supplemented with $TiO_2$ nanoparticle concentrations between 0.5 μg/mL and 10,000 μg/mL added.

Control groups included untreated MG-63 cells (no inoculation with $TiO_2$) and cells treated with 250 μM Triton X-100 (VWR, Dorset, UK).

MTT assays were performed as previously reported [28]. Briefly, MTT salt solution (5 mg/mL) was added 5 h prior to the end of the 24 h $TiO_2$ nanoparticle incubation to allow cellular tetrazolium metabolism. After 5 h DMSO (Sigma-Aldrich, Steinheim, Germany) was added to solubilise formazan crystals, and absorption was measured using a microplate reader (Anthos 2020, Anthos Labtec, Wals/Salzburg, Austria) at a wavelength of 570 nm with a reference wavelength of 620 nm.

### 2.7 Statistical analysis

MTT experiments were repeated three times. The percentage mitochondrial respiratory activity (viability of MG-63 osteoblast-like cells) was expressed as average values ± standard deviation for each group of cells (untreated cells, cells treated with $TiO_2$ nanoparticles, cells treated with Triton X). Differences between the treated groups and the untreated cells (control) were assessed by one-way variance analysis (ANOVA) followed by Dunnett test. Statistical significance was measured at a probability $p<0.05$.

## 3 Results

### 3.1 Morphology of the as-prepared composite films

SEM micrographs of the PDLLA film containing no titanium dioxide nanoparticles (Fig. 1a) had a smooth surface with no evidence of surface topography. The composite of PDLLA film incorporated with 5 wt% $TiO_2$ (Fig. 1b) shows an evenly distribution of $TiO_2$ nanoparticles with few agglomerates. Similarly, the PDLLA composite filled with 30 wt% $TiO_2$ (Fig. 1c) has an even distribution of nanoparticles but there are also some large agglomerates of titanium dioxide present. The SEM micrographs of the composite films also indicate that the titanium dioxide nanoparticles are not directly exposed on the composite surface but rather embedded in the PDLLA matrix.

It can be qualitatively noted that an increasing percentage of $TiO_2$ nanoparticles present in the composites results in rougher surfaces as well as greater fracture surface areas. This observation was corroborated by surface characterisation via white light interferometry (Zygo$^{TM}$). There is a notable increase in the average surface roughness, characterised by the parameter $R_a$, with $R_a = 3.51$ for the composite film with

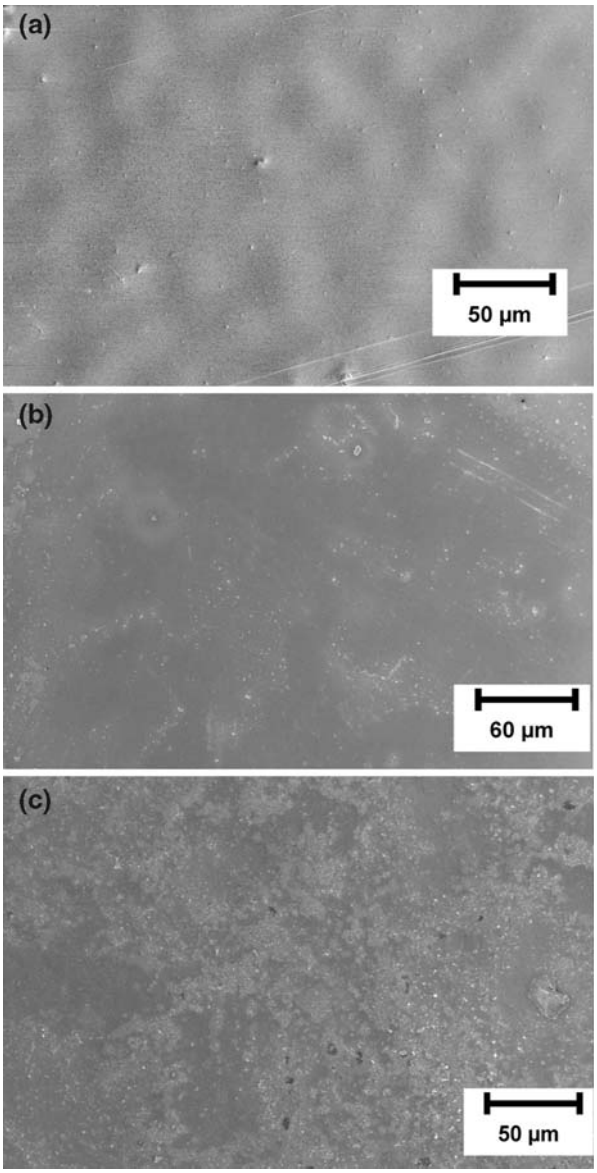


**Fig. 1** SEM micrographs of as-prepared PDLLA films: (**a**) without $TiO_2$ nanoparticles, (**b**) containing 5 wt% $TiO_2$ nanoparticles, and (**c**) containing 30 wt% $TiO_2$ nanoparticles. A smooth surface can be observed in (a). Film roughness increases with increasing concentration of $TiO_2$ nanoparticles

30 wt% $TiO_2$ nanoparticles compared to $R_a = 0.86$ for films with 5 wt% $TiO_2$ (Fig. 2) and $R_a = 0.63$ for the pure PDLLA sample. In other words, the PDLLA films containing 30 wt% $TiO_2$ possess 4 times and 5.6 times higher roughness value, compared to the low content (5 wt% $TiO_2$) and pure PDLLA films, respectively.

Fracture surfaces of composite films containing either 5 or 30 wt% $TiO_2$ showed relatively well distributed titanium dioxide nanoparticles throughout the approximately 10–15 μm thick PDLLA film matrix,

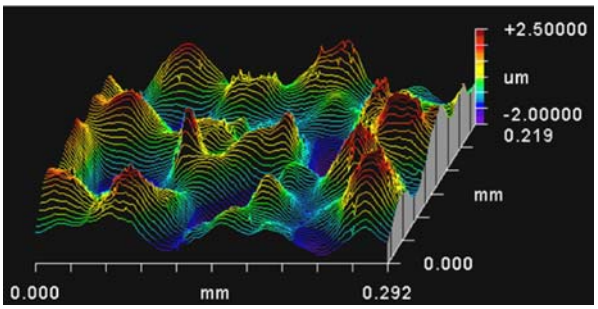


**Fig. 2** Surface profile of a PDLLA composite film containing 5 wt% $TiO_2$. The profile exemplarily shows the interferometric roughness measurement ($R_a$ = 0.86) obtained from a surface area of 0.29 mm × 0.22 mm

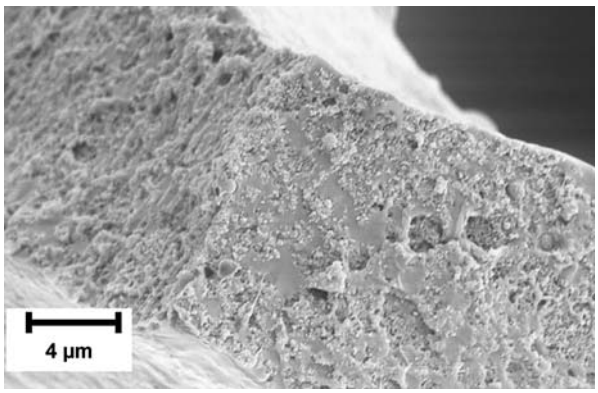


**Fig. 3** SEM micrograph showing the fracture surface of a PDLLA composite film with 30 wt% $TiO_2$. The fracture surface exhibits $TiO_2$ particle debonding

as shown in Fig. 3 for the composite film with 30 wt% $TiO_2$. The fracture surfaces also exhibited a rough appearance due to the nanoparticles being debonded from and pulled out of the matrix. This shows that the method of incorporating titanium dioxide into the PDLLA matrix was successful and confirmed that nanoparticles were fully embedded in the polymer. It also demonstrates that the interfaces between $TiO_2$ nanoparticles and PDLLA matrix are relatively weak. This should have implications on the mechanical properties of the composites. For example, particle debonding due to weak particle/matrix interface can activate toughening mechanisms required to increase fracture toughness [29].

### 3.2 Possible bioactivity of PDLLA/$TiO_2$ composites and $TiO_2$ nanoparticles

The bioactive behaviour of the films was assessed by immersion in 1.5 SBF for different periods of time. The composite films were characterised after immersion in 1.5 SBF for 4, 7, 14 and 21 days. Possible formation of stoichiometric or non-stoichiometric HA was assessed and monitored by observing the Raman peak at wavenumber 960–963 $cm^{-1}$ as a function of immersion time. Results of the Raman spectroscopy investigations are shown in Figs. 4 and 5.

Raman spectroscopy revealed no clear evidence of HA crystal formation following short-term immersion periods, i.e., after 4 and 7 days, in samples exposed to 1.5 SBF. Some trace amounts of non-stoichiometric HA may be present after 7 days on the PDLLA film containing 30 wt% $TiO_2$ nanoparticles as a small peak at 961 $cm^{-1}$ was occasionally observed. Thus, nucleation of HA crystals has possibly taken place after 7 days of immersion in 1.5 SBF in composite films containing 30 wt% $TiO_2$. There was clear evidence of

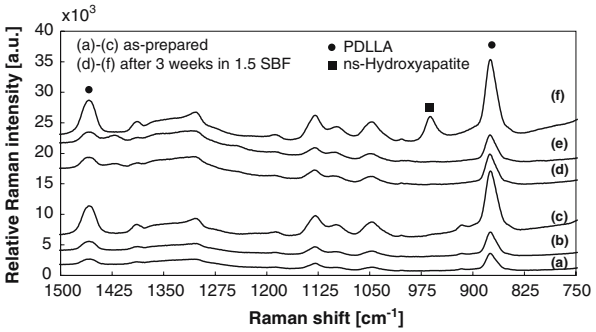


**Fig. 4** Raman spectra of different films investigated. (**a**) As-prepared PDLLA film, (**b**) as-prepared PDLLA film containing 5 wt% $TiO_2$, (**c**) as-prepared PDLLA film containing 30 wt% $TiO_2$, (**d**) PDLLA film after 3 weeks in 1.5 SBF, (**e**) PDLLA film containing 5 wt% $TiO_2$ and (**f**) PDLLA film containing 30 wt% $TiO_2$ after 3 weeks in 1.5 SBF. Only in the latter spectrum (f) there is evidence of ns-HA due to a distinctive peak at 961 $cm^{-1}$ [30, 31]. For all other samples the apparent characteristic peaks of PDLLA can be observed at 875 and 1452 $cm^{-1}$ [32, 33]. The spectra are average spectra obtained from five different locations on the films

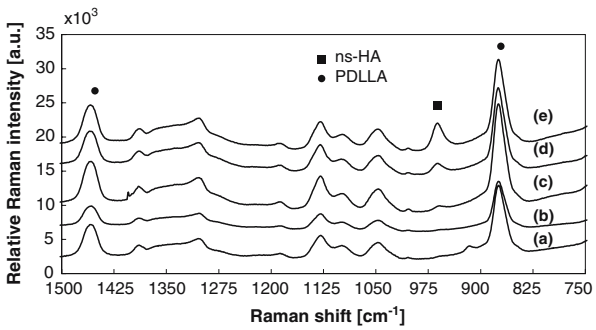


**Fig. 5** Time dependent formation of HA on PDLLA films containing 30 wt% $TiO_2$: (**a**) as-prepared, (**b**) after 4 days, (**c**) after 7 days, (**d**) after 14 days, (**e**) after 21 days of incubation in supersaturated SBF. The greatest change occurs between 7 days and 14 days where formation of ns-HA was triggered

apatite structure after 14 days and 21 days for the PDLLA film containing 30 wt% $TiO_2$ as shown in Fig. 5, whilst no HA formation was observed for the entire incubation period when pure PDLLA samples were studied in the same conditions. Moreover, some trace amounts of HA were detected even for the low content $TiO_2$ composite film (5 wt%), after immersion periods of 14 and 21 days (results not shown).

As mentioned above, characteristic HA Raman peaks were observed at 961 $cm^{-1}$; which indicates that non-stoichiometric HA (ns-HA) crystals have been formed on the surfaces of the PDLLA-based films. Stoichiometric HA has a distinctive peak at 963 $cm^{-1}$ whereas non-stoichiometric HA mineral (e.g., in bone) exhibits a vibrational Raman peak at 961 $cm^{-1}$ [30, 31]. The stretching of the phosphate ($PO_4$) band at 960 $cm^{-1}$ shifts slightly from the respective band of stoichiometric HA (963 $cm^{-1}$) possibly due to carbonate $(CO_3)^-$ substitution or other ions/substitutes (e.g., Mg, $Cl^-$) coming from the SBF solution. This happens also often in normal bone where the channel site, i.e., the hydroxy group $(OH)^-$ of $Ca_{10}(PO_4)6(OH)_2$, can be occupied by several ions leading to non-stoichiometry. Substitutional sites in the HA structure $(Ca_{10}(PO_4)_2(OH)_2$ can be occupied not only by $OH^-$, but also by other ions (e.g., $Cl^-$, $Mg^{2+}$) leading to non-stoichiometry. Characteristic peaks of PDLLA can be observed at 875 and 1452 $cm^{-1}$ [32, 33]. The 875 $cm^{-1}$ peak corresponds to –C–C stretching [32, 33], and the 1452 $cm^{-1}$ is related to antisymmetric bending of the $–CH_3$ (methyl) band. A time dependant formation of HA on the surface of the PDLLA films containing 30 wt% $TiO_2$

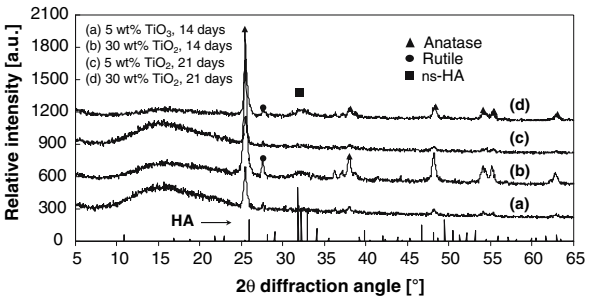


**Fig. 6** XRD patterns of PDLLA films containing 5 wt% and 30 wt% $TiO_2$ nanoparticles after immersion in 1.5 SBF for 14 days (**a**, **b**) and 21 days (**c**, **d**), respectively. There is no evidence of HA formation after 14 days when comparing the patterns with the reference spectrum of HA (also shown in the figure). The only peaks observed are those corresponding to the phases of the starting $TiO_2$ material (anatase and rutile). However, for the films containing 30 wt% $TiO_2$ nanoparticles, after immersion in 1.5 SBF for 14 and 21 days, there is a broad HA peak at the $2\theta$ diffraction angle of 32° [34]. The broad bumps between $2\theta$ diffraction angles of 10 and 25° are due to the amorphous PDLLA matrix

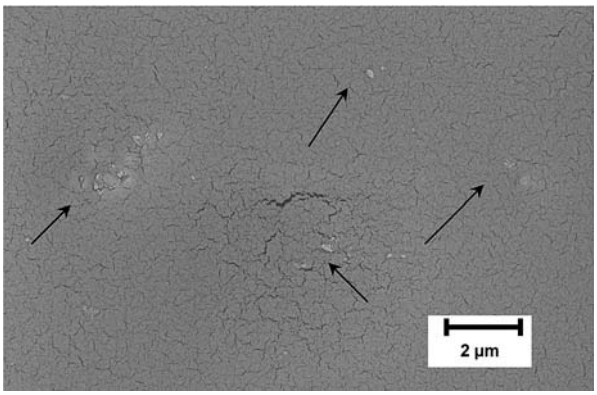


**Fig. 7** SEM micrograph of a film containing 5 wt% $TiO_2$ nanoparticles after 21 days immersion in 1.5 SBF. The film exhibits some trace amounts of HA crystals (small white spots), attached and irregularly distributed on the film surface. The cracks visible within the polymer matrix are artefacts due to the electron beam. The arrows indicate the small HA crystals. A similar surface topography was observed for pure PDLLA films after 21 days immersion in 1.5 SBF

was observed (Fig. 5). The distinct ns-HA peak [30] (wavenumber 961 $cm^{-1}$) increased with time. There was a progressive HA formation from day 14 to day 21 of incubation, as shown in Fig. 5.

The XRD pattern for the composite film containing 30 wt% $TiO_2$ after 14 and 21 days of incubation in 1.5 SBF showed a broad peak at the $2\theta$ diffraction angle of 32°, which is typical for poorly crystalline HA (Fig. 6) [34]. This finding differs from results on the film containing 5 wt% for which no crystalline peaks of HA were observed after 14 and 21 days of immersion in 1.5 SBF.

SEM examination of all tested samples (0, 5 and 30 wt% $TiO_2$) indicated changes in the appearance and morphology (microstructure) of the films after 14 and 21 days of incubation in 1.5 SBF. SEM images revealed some small HA crystals on the surface of the pure PDLLA film and of the low content (5 wt% $TiO_2$) PDLLA film after 21 days of immersion in 1.5 SBF (Fig. 7), which had not been detected by Raman spectroscopy. This discrepancy is probably due to the Raman spectroscopy sampling method and the heterogeneous distribution HA crystals on the film surface.

SEM examination of 30 wt% $TiO_2$ containing samples after immersion in 1.5 SBF clearly indicated formation of HA crystals after 14 and 21 days (Fig. 8), as detected by Raman spectroscopy and XRD analysis. The comparison of Fig. 8a and b qualitatively indicates a trend of increasing HA formation from day 14 to day 21 of incubation. Although HA formation is more dispersed on the image in Fig. 8b, the overall amount of HA in both images does not apparently seem significantly distinct. However,

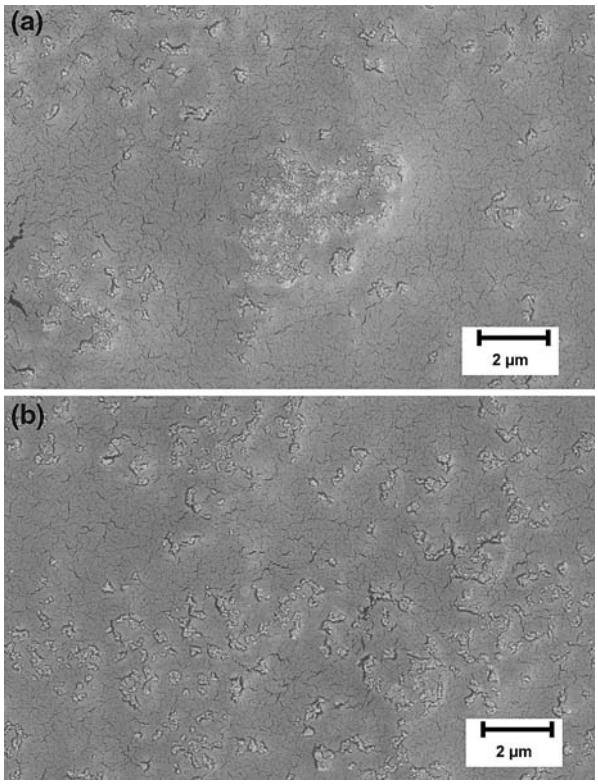


**Fig. 8** Progressive formation of HA on the surface of PDLLA films containing 30 wt% $TiO_2$ nanoparticles after exposure to 1.5 SBF, *qualitatively assessed by visual inspection.* (**a**) A large agglomeration as well as small HA crystals are apparent after 14 days. (**b**) A homogeneous formation of HA crystals covers the film surface after 21 days. The visible cracks are artefacts due to damage to the films during SEM observation

Raman spectra obtained on five different locations have indicated a progressive formation of HA between 14 and 21 days incubation, as reported in Fig. 5.

Moreover, a homogeneous distribution of HA crystals with an average particle size of approximately 40 nm was observed on the 30 wt% $TiO_2$ containing film after 14 days incubation as Fig. 9 shows. The formed crystals seem to be well bonded to the film surface and somewhat embedded into the polymer matrix. The surface in Fig. 9 appears considerably rougher compared to the untreated film with the same percentage (30 wt%) of $TiO_2$ (as shown in Fig. 1c), due to the presence of HA nanocrystals. This local nanotopography should have a positive effect regarding adhesion of osteoblast cells, according to the literature [14, 15].

The chemical composition of the observed crystals was assessed by an Energy Dispersive Spectrometer (EDS) (INCA EDS system 430, Oxford Instruments, Santa Clara, California, USA). EDS was performed to analyze the composition of the crystals formed on the

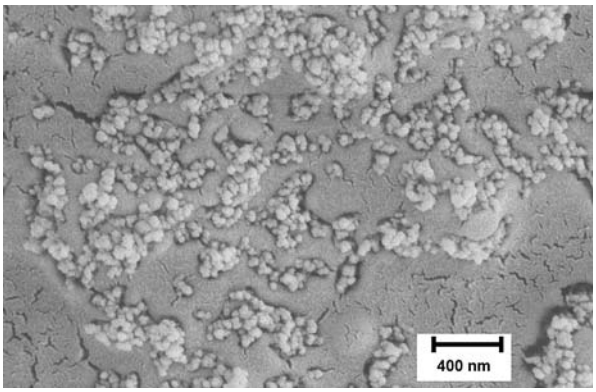


**Fig. 9** SEM micrograph showing well distributed HA nanocrystals with an estimated average diameter of 40 nm after 14 days of incubation in 1.5 SBF on a 30 wt% $TiO_2$ containing film. The crystals seem to be well-bonded to and partially embedded in the matrix due to the shadow surrounding the crystals

30 wt% $TiO_2$ containing sample which are clearly visible in the SEM micrograph (Fig. 9). Figure 10 shows the EDS spectrum of the crystals, which have the typical morphology of HA. The results confirmed a considerable amount of calcium (Ca) present. However, due to the gold coating used for the preparation of the samples for SEM–EDS analysis, the characteristic phosphorus peak at X-ray energy of 2.05 keV is overlapped by the strong gold signal in this energy region.

The bioactivity of as-received $TiO_2$ nanoparticles was investigated by immersing the powder in 1.5 SBF for 21 days. Possible HA formation was examined by Raman spectroscopy. The Raman spectra (results not presented here) showed no evidence of the characteristic HA peaks at the Raman spectrum shift 961–963 $cm^{-1}$ for the complete duration of the experiment

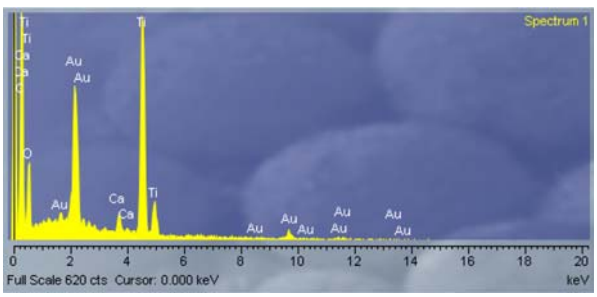


**Fig. 10** EDS spectrum recorded on the region considered to be HA crystals in Fig. 9. There is evidence of considerable amount of calcium (Ca), one of the elements in HA. The strong signals of titanium (Ti) and gold (Au) come from the $TiO_2$ particles and the gold coating used for sample preparation, respectively. The characteristic phosphorus peak of HA occurs at X-ray energy of 2.05 keV and it is overlapped by the strong gold signal in this energy region

(21 days). A possible reason could be that the particles have sedimented on the bottom of the tube and provided only a small surface area for HA nucleation. To optimise the setup for testing particle bioactivity in SBF or other relevant fluids it is recommended to circulate the nanoparticles in a closed circuit which should lead to a considerably larger surface area for contact with SBF [35].

### 3.3 Cell morphology and MTT assay

MG-63 cells incubated with $TiO_2$ nanoparticles (5 μg/mL) had a similar morphology and confluence level to control cell after 24 h (Fig. 11). $TiO_2$ particle agglomerations were also visible in treated MG-63 cells due to clumping in the cell culture medium.

MTT assays revealed decreasing cell viability with increasing $TiO_2$ concentration (Fig. 12). Low concentrations of $TiO_2$ nanoparticles (0.5–10 μg/mL) had no significant effect on cell viability. At high $TiO_2$ nanoparticle concentrations the nanoparticles induced a considerable cytotoxic effect with viabilities of 49% ± 4% and 38% ± 3% observed for particle concentrations of 5000 and 10,000 μg/mL, respectively.

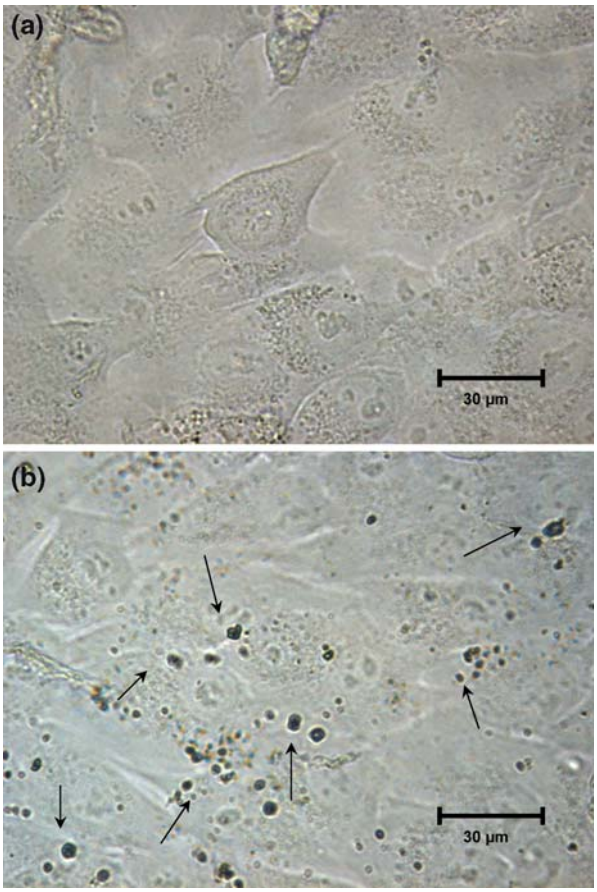


**Fig. 11** MG-63 osteoblast-like cells after 24 h seeded in a 96-well with a density of 10,000 cells/well; (**a**) untreated cells, flattened and well spread cells can be observed, (**b**) cells treated with $TiO_2$ nanoparticles (5 μg/mL), a similar cell morphology is apparent as well as a few areas with large $TiO_2$ agglomerations indicated by arrows

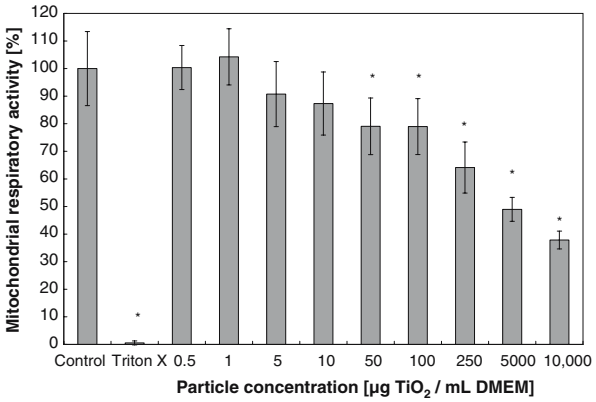


**Fig. 12** The effect of 24 h $TiO_2$ nanoparticle challenge on MG-63 metabolic activity as measured by MTT assay. The data represent average values from three different and independent tests. Asterisks (*) indicate the significant difference from the control (untreated cells) at $p < 0.01$

## 4 Discussion

The osteoconductivity and mechanical integrity of bone analogue materials and bone tissue engineering scaffolds can potentially be enhanced by the growth of non-stoichiometric, bone-like HA crystals on their surfaces [36]. The formation of HA crystals on the material surface is considered a measure of the bioactivity of the scaffolds, such as investigated in this study for PDLLA/$TiO_2$ composite films. Moreover, the addition of ceramic nanoparticles to polymer matrices has been previously shown to enhance osteoblast cell adhesion [16, 18–20].

PDLLA/$TiO_2$ composites exhibited increasing surface roughness with increasing titanium dioxide nanoparticle content. Compared to the pure PDLLA films (containing no $TiO_2$ nanoparticles), there is a 557% greater surface roughness for the PDLLA films with 30 wt% $TiO_2$, as measured by the average surface roughness parameter $R_a$ (Fig. 2). It has been reported that bulk $TiO_2$ substrates processed with nanoparticles have approximately 35% more surface area compared to the respective conventional materials (made with $TiO_2$ particles of size >100 nm), leading to a 30% greater osteoblast adhesion [13, 14]. The present study provides evidence of the formation of non-stoichiometric HA (ns-HA) crystals in nanometre dimensions

(~40 nm) on surfaces of PDLLA films containing 30 wt% $TiO_2$ upon immersion in 1.5 SBF after 7 days. A large density of crystals with a homogeneous crystal distribution was achieved after 14 and 21 days of immersion in 1.5 SBF. HA nanocrystals with grain sizes <100 nm possess the ability to simulate the nanometre surface roughness found in osseous tissue [6] leading to enhanced scaffold and implant performance, i.e., improved material/tissue interaction and adhesion [21–23]. Even if the initial polymer weight to solvent ratio in this study was slightly higher than in the previous study (5% vs. 4% (w/v) [25]), the main difference between both investigations was the use of different solutions (concentrated 1.5 SBF vs. SBF), which led to the different bioactivity results.

In this investigation, HA formation on PDLLA/$TiO_2$ composites was triggered and accelerated by using supersaturated SBF with ion concentrations 1.5 times those of SBF, a process known in literature as the ''biomimetic process'' [21–24]. The combination of PDLLA and $TiO_2$ allows two possible reactions leading to surface nucleation and subsequent mineral (apatite) growth. HA formation on the composite surfaces can be triggered by the surface condition of both the PDLLA polymer and the titanium dioxide particles. Therefore two different routes or mechanisms of HA formation can be suggested, as discussed next.

Firstly it could be expected that PDLLA surfaces are hydrolysed by water molecules in 1.5 SBF, which convert ester linkages into surface carboxylic groups (COOH). At physiological pH 7.25 the COOH groups should dissociate into carboxylate anions ($COO^-$), which provide a negatively charged surface for binding of calcium ions ($Ca^{2+}$). The affiliation and binding of these ions stimulates surface nucleation with subsequent HA crystal growth, similar to the mechanism proposed by Murphy et al. [36].

Secondly a similar reaction path is conceivable due to the presence of titanium dioxide nanoparticles within the polymer matrix. $TiO_2$ is able to absorb water at the surface, resulting in titanium hydroxide (Ti–OH) groups [37]. In the buffered and neutral supersaturated SBF solution (pH 7.25), the Ti–OH groups dissociate leading to a negatively charged $TiO_2$ surface that provides sites for calcium phosphate nucleation [38, 39]. This mechanism has been proposed for sol-gel derived $TiO_2$ gels and films [38–40], however it has not been proven in $TiO_2$ nanoparticles. Furthermore, it has been reported that Ti–OH groups in $TiO_2$ gels are particularly effective in inducing apatite formation if $TiO_2$ is present in its anatase modification [40]. The $TiO_2$ powder used in this study consists of approximately 80% anatase modification, this considerable amount of anatase may thus have promoted and contributed to the progressive HA formation on the PDLLA film containing 30 wt% $TiO_2$, as documented in Figs. 8 and 9.

We suggest that both reaction paths are conceivable in our composites, and evidence is given by the fact that some HA (ns-HA) crystals have been found on the pure PDLLA films after 21 days of immersion in 1.5 SBF. In a previous investigation using similar composites but immersion in standard simulated body fluid, no evidence of HA formation was detected upon 21 days immersion in SBF [25]. By using supersaturated SBF in this study, it can be assumed that nucleation and growth of ns-HA nanocrystals was accelerated due to the higher concentration of the relevant ions in contrast to standard SBF. As described above, the formed ns-HA nanocrystals seem to bind strongly to the composite films surface and are somewhat embedded into the PDLLA/$TiO_2$ substrate. This behaviour is beneficial compared to HA coatings deposited from an external source, for example by spraying or sputtering techniques, as the quality of these coatings frequently varies because of poor adhesion between the coating and the substrate [41].

The hypothesis that crystals observed on surfaces of PDLLA/$TiO_2$ films are composed of non-stoichiometric HA as suggested here might be supported by the recent investigation by Pasteris et al. [42]. In their investigation several biological apatites as well as synthetic HA were characterised by Raman spectroscopy and it was shown that OH-incorporation into the apatite crystal lattice is reduced for nanocrystallite biological apatites, such as those found in bone and dentin. It is believed that the lack of OH– in bone apatite has a physiological purpose: e.g., non-stoichiometric bone apatite (Ca/P ratio <1.67) contains additional substitutes, such as magnesium, carbonate or chloride ions, leading to a higher apatite solubility which facilitates metabolism and the bone remodelling process [42].

In our study the ''biomimetic process'' (immersion of samples in 1.5 SBF) was utilised to trigger and accelerate apatite formation on PDLLA/$TiO_2$ composites. Formation of HA nanocrystals on the PDDLA/$TiO_2$ composites was confirmed by Raman spectroscopy and XRD measurements. The degree of crystallinity and how close the observed HA crystals are to stoichiometric HA is still to be investigated by assessing the Ca/P ratio in the crystals formed. The exact mechanism of HA formation on surfaces is still not fully understood. Besides well-known effects of the chemistry of PDLLA and $TiO_2$ nanoparticles as well as

the higher concentrations of relevant ions in 1.5 SBF (in particular $Ca^{2+}$, $HPO_4^{2-}$) more factors should contribute to apatite formation, such as: surface area, topographic features, microcracks, and porosity of the films. Indeed the more than 5 times greater surface area of the 30 wt% $TiO_2$ films should have promoted increased apatite formation and thus surface area is considered a key factor in the HA formation process. Moreover, the surface microstructure of the PDLLA-based films might also change during the soaking period in supersaturated SBF. In fact the macroscopic appearance of the pure PDLLA film and the 5 wt% $TiO_2$ film after immersion in 1.5 SBF showed a rougher surface with small bubbles and pits. This is in contrast to the film containing 30 wt% $TiO_2$ which looked very similar (under SEM) to the as-prepared composite film even after a degradation period of 21 days.

Nanostructured composites on the basis of bioresorbable polymers and ceramic nanoparticles may possess the ability to simulate surface and/or chemical properties of bone, allowing for exciting alternatives in the design of prosthesis as well as scaffolds with greater efficacy and performance [15–20]. Advantages and benefits of nanophase ceramics in bone tissue engineering applications have been documented in literature [13–20]. Greater osteoblast adhesion, greater alkaline phosphatase (ALP) synthesis (biochemical marker for bone metabolism), as well as enhanced concentration of calcium in the extracellular matrix were observed compared to conventional (micrometer) ceramics when using nanoparticles either as bulk material or as filler for polymer matrices. However, it must be emphasised that enhanced in vitro performance (e.g., cell adhesion) does not necessarily mean better in vivo performance of biomaterials. Therefore, prolonged in vitro and in vivo degradation studies are suggested to be performed in future in order to investigate how the degradation of the polymer affects the local nanoparticle concentration, which should have an effect on the behaviour of the adjacent cells and tissues.

In this investigation, composite films were developed using amorphous PDLLA. There are some remarkable and beneficial properties associated with PDLLA as composite matrix material. It has been reported that PDLLA implants have been completely resorbed from the extracellular space in animal studies with a maximum drop in pH of 0.1 units in the immediate implant environment [43]. Furthermore, PDLLA degraded without any crystalline remnants. Crystalline remnants of PLLA bone plates and screws have been considered to be responsible for late inflammation (swelling) and foreign body reactions at the site of implantation [44].

The findings in this work imply that $TiO_2$ nanoparticles embedded into a PDLLA matrix could represent a potential improved substitution for micrometer size ceramic particles which are currently used as fillers in bioresorbable polymer scaffolds [4, 5, 45]. However, a potential negative effect of nanoparticle-containing scaffolds is the possibility of migration of nanoparticles within the body and their distribution via blood stream, leading to pathologies of unknown origin (nanopathologies) [46]. For example, pro-inflammatory effects on endothelial cells [47] as well as the enhanced free radical activity of nanoparticle surfaces which is able to cause DNA strand breakage [48] must be carefully taken into consideration.

As indicated above, ceramic nanoparticles have been shown in previous studies to have different effects on cellular behaviour than larger (conventional) particles of micrometer dimensions [13–20, 49]. In the present study, to understand how free $TiO_2$ nanoparticles (released from the PDLLA matrix) might modulate osteoblast activity, the response of MG-63 osteoblast-like cells to nanoparticles was examined. It has been recently shown in a simulated wear debris study that osteoblasts exhibit a more well-spread morphology and increased viable cell density in the presence of $TiO_2$ and $Al_2O_3$ nanoparticles compared to micrometer sized particles [20]. In the present study, low concentrations of $TiO_2$ nanoparticles (0.5–10 μg/mL) had no significant effect on MG-63 cell mitochondrial respiratory rates. Stepwise decreasing viability can be observed with increasing particle concentrations greater than 50 and 250 μg/mL to a final viability of 38% ± 3% for a $TiO_2$ nanoparticle concentration of 10,000 μg/mL (Fig. 12). However, concentrations greater than 100 μg/mL may be not considered physiologically relevant by comparing for example wear debris rates from aseptic loosened ceramic on ceramic bearings. In prolonged degradation studies, research should also be carried out to characterise release profiles of the $TiO_2$ nanoparticles generated following the polymer matrix degradation. It must be assured and proven that local $TiO_2$ nanoparticle concentrations in tissues do not exceed a safe level, which should be of the order of 100 μg/mL for the used titania nanoparticles, as found in this study.

On the basis of data on volumetric annual wear of 1 $mm^3$ [50], ceramic exposure of tissues and cells in rates of approximately 10 μg per day (i.e., $5.7 \times 10^{11}$ particles per day) can be considered as physiologically relevant, and this was taken as an indication for the present cell culture experiments with $TiO_2$ nanoparticles. The amount of ceramic debris was calculated by assuming spherical $TiO_2$ particles and taking into

account the density of $TiO_2$ as well as primary particle diameter.

For high particle concentrations (5000 and 10,000 μg/mL) the present osteoblast viabilities differ considerably from literature values. Gutwein and Webster have reported bone-derived osteoblast viabilities of about 15% and 8% after treatment with $TiO_2$ nanoparticles in concentrations of 5500 and 10,000 μg/mL, respectively for 6 h [20]. For the same concentrations, the present results showed a viability of 49% ± 4% and 38% ± 3% after 24 h of inoculation of MG-63 cells with $TiO_2$ nanoparticles. These differences could be explained by cell type, seeding densities and viability test method. On the other hand, the present MG-63 viability study following nanoparticle exposure is in accordance with recent studies where human osteoblasts challenged with $Al_2O_3$ and UHMWPE micrometer particles were found to be unaffected by debris concentrations at 1–10 μg/mL [51].

To the authors' knowledge there are only a few investigations dealing with the assessment of cytotoxic effects of ceramic nanoparticles during simulated in vivo wear [17, 20, 52]. There is evidence that particles with smaller diameters have less detrimental effects on cells [17]. Moreover, it has previously been reported that for phagocytosable particles (i.e., particles <3 μm in diameter which can be internalised by cells via phagocytosis [53]) increasing the size of particle correlates with increasing cytotoxicity [17]. However, the cellular responses to ceramic nanoparticles depend on several factors including particle shape, chemical stability as well as mechanical stimulation, which influence the cellular behaviour and the particle cytotoxicity. This study conclusively showed that $TiO_2$ nanoparticle concentrations of up to 10 μg/mL do not affect cell osteoblast viability, which may have important implications for the use of titanium dioxide nanoparticles for designing novel resorbable matrix composite scaffolds. However $TiO_2$ nanoparticles may also cause phenotypic changes in the cells (e.g., the release of cytokines and proteases), which may effect osteoblast differentiation, osteoblast recruitment and matrix formation possibly resulting in decreased bone forming ability [15, 54].

As a final note, we would like to point out that steam sterelisation, as used in this study, might have been a significant factor affecting the results. Possible effects of steam sterilisation on the nanoparticles, which are not known, must be taken into account in any future related study. $TiO_2$ nanoparticles might react with steam to form Ti–OH groups on the surface. As a result, steam sterilisation may modify the composition, surface structure and properties of the $TiO_2$ nanoparticles.

## 5 Conclusions

Poly(D,L lactid acid) composite films were successfully manufactured by solvent casting with different percentages of titanium dioxide nanoparticles (5 and 30 wt%) and a relatively homogeneous distribution of $TiO_2$ nanoparticles in the PDLLA matrix was achieved. The increase in nanoparticles content increased the surface roughness of the films, which may improve adhesion of osteoblast cells. It was found that homogeneously distributed non-stoichiometric HA nanocrystals formed on the high content (30 wt% $TiO_2$) composite film after 14 and 21 days of immersion in 1.5 SBF. For the pure PDLLA films and the low content composite films (5 wt% $TiO_2$) trace amounts of non-stochiometric HA are apparent after 21 days immersion according to SEM micrographs. The titanium dioxide nanopowder itself showed no bioactivity. The formation of HA was confirmed by SEM–EDS, Raman spectroscopy and XRD analyses. This study also showed that $TiO_2$ nanoparticles in physiological relevant range (≤100 μg/mL) had no significant effect on MG-63 osteoblast-like cell viability. Taken the main findings of this work in consideration, titanium dioxide nanoparticles emerge as promising filler material to be used for designing tissue engineered constructs (composite scaffolds) based on degradable polymer matrices. A major challenge for the future is to create three dimensional structures with interconnective pores to use these composites as scaffolds in bone tissue engineering for regenerating diseased or damaged bone tissue such as trauma, congential defects, cancer or other bone diseases.

**Acknowledgments** The authors gratefully acknowledge the experimental assistance and expertise of I. Notingher, M. Ardakani, M. Kershaw, R. Chater (all Department of Materials, Imperial College London, UK). The authors would also like to thank T. Kasuga (Department of Materials Science and Engineering, Nagoya Institute for Technology, Japan) for helpful discussions as well as Professor L.L. Hench (Department of Materials, Imperial College London, UK) for funding the cell biological experiments. Thanks are also due to the German Academic Exchange Service (DAAD) for funding provided for L.-C. Gerhardt.

## References

1. C. E. HOLY, M. S. SHOICHET and J. E. DAVIES, *J. Biomed. Mater. Res.* **51** (2000) 376
2. J. M. TABOAS, R. D. MADDOX, P. H. KREBSBACH and S. J. HOLLISTER, *Biomaterials* **24/1** (2003) 181
3. I. D. THOMPSON and L. L. HENCH, *Proc. Inst. Mech. Eng. [H]* **212/2** (1998) 127
4. S. RAMAKRISHNA, J. MAYER, E. WINTERMANTEL and K. W. LEONG, *Comp. Sci. Technol.* **61/9** (2001) 1189

5. A. R. BOCCACCINI and V. MAQUET, *Comp. Sci. Technol.* **63/16** (2003) 2417
6. C. LOTY, J. M. SAUTIER, H. BOULEKBACHE, T. KOKUBO, H. M. KIM and N. FORST, *J. Biomed. Mater. Res.* **49** (2000) 423
7. L. L. HENCH and J. K. WEST, *Life Chem. Rep.* **13** (1996) 187
8. J. R. JONES and L. L. HENCH, *Mat. Sci. Technol.* **17/8** (2001) 891
9. T. W. BAUER, *Clin. Orthop.* **405** (2002) 138
10. T. W. BAUER and J. SCHILS, *Skeletal Radiol.* **28/9** (1999) 483
11. P. A. REVELL, N. AL-SAFFAR and A. KOBAYASHI, *Proc. Inst. Mech. Eng. [H]* **211** (1997) 187
12. R. W. SIEGEL, *Sci. Am.* **275** (1996) 42
13. T. J. WEBSTER, *Am. Ceram. Soc. Bull.* **82/6** (2003) 23
14. T. J. WEBSTER, R. W. SIEGEL and R. BIZIOS, *Biomaterials* **20/13** (1999) 1221
15. J. K. SAVAIANO and T. J. WEBSTER, *Biomaterials* **25/7–8** (2004) 1205
16. S. KAY, A. THAPA, K. M. HABERSTROH and T. J. WEBSTER, *Tissue Eng.* **8/5** (2002) 753
17. A. YAMAMOTO, R. HONMA, M. SUMITA and T. HANAWA, *J. Biomed. Mater. Res.* **68A/2** (2004) 244
18. T. J. WEBSTER, C. ERGUN, R. H. DOREMUS, R. W. SIEGEL and R. BIZIOS, *Biomaterials* **21/17** (2000) 1803
19. T. J. WEBSTER, C. ERGUN, R. H. DOREMUS, R. W. SIEGEL and R. BIZIOS, *J. Biomed. Mater. Res.* **51**(3) (2000) 475
20. L. G. GUTWEIN and T. J. WEBSTER, *Biomaterials* **25/18** (2004) 4175
21. P. ZHU, Y. MASUDA and K. KOUMOTO, *Biomaterials* **25/17** (2004) 3915
22. R. ZHANG and P. X. MA, *J. Biomed. Mater. Res.* **45/4** (1999) 285
23. X. YUAN, A. F. MAK and J. LI, *J. Biomed. Mater. Res.* **57/1** (2001) 140
24. H. K. VARMA, Y. YOKOGAWA, F. F. ESPINOSA, Y. KAWAMOTO, K. NISHIZAWA, F. NAGATA and T. KAMEYAMA, *Biomaterials* **20/9** (1999) 879
25. A. R. BOCCACCINI, L.-C. GERHARDT, S. REBELIN and J. J. BLAKER, *Composites Part A* **36/6** (2005) 721
26. M. ETTLINGER, Fine Particles, in Technical Bulletin Pigments, No. 80. Degussa AG, Inorganic Chemical Products Division: Düsseldorf, pp. 1–26
27. T. KOKUBO, H. KUSHITANI, S. SAKKA, T. KITSUGI and T. YAMAMURO, *J. Biomed. Mater. Res.* **24/6** (1990) 721
28. T. MOSMANN, *J. Immunol. Methods* **65/1–2** (1983) 55
29. F. L. MATTHEWS and R. D. RAWLINGS, Composite materials: Engineering and science, ed. Woodhead Publishing Ltd, Cambridge, UK (1999), pp. 342–354
30. G. PENEL, G. LEROY, C. REY and E. BRES, *Calcif. Tissue Int.* **63/6** (1998) 475
31. G. PENEL, G. LEROY, C. REY, B. SOMBRET, J. P. HUVENNE and E. BRES, *J. Mater. Sci. Mater. Med.* **8/5** (1997) 271
32. G. KISTER, G. CASSANAS and M. VERT, *Polymer* **39/15** (1998) 3335
33. P. TADDEI, A. TINTI and G. FINI, *J. Raman Spectr.* **32/8** (2001) 619
34. ICDD, Powder Diffraction File, Inorganic Volume: Sets 9, 21, International Centre for Diffraction Data, I. Editor, ed., Swarthmore, Pennsylvania, USA 1967 (set 9), 1980 (set 21), pp. 9–432, 21–1271, 21–1276
35. A. RAMILA and M. VALLET-REGI, *Biomaterials* **22/16** (2001) 2301
36. W. L. MURPHY, D. H. KOHN and D. J. MOONEY, *J. Biomed. Mater. Res.* **50/1** (2000) 50
37. H. P. BOEHM, *Discuss. Faraday Soc.* **52** (1971) 264
38. H. MAEDA, T. KASUGA and M. NOGAMI, *J. Eur. Ceram. Soc.* **24/7** (2004) 2125
39. T. PELTOLA, M. JOKINEN, H. RAHIALA, E. LEVANEN, J. B. ROSENHOLM, I. KANGASNIEMI and A. YLI-URPO, *J. Biomed. Mater. Res.* **44/1** (1999) 12
40. M. UCHIDA, H. M. KIM, T. KOKUBO, S. FUJIBAYASHI and T. NAKAMURA, *J. Biomed. Mater. Res.* **64A/1** (2003) 164
41. X. ZHENG, M. HUANG and C. DING, *Biomaterials* **21/8** (2000) 841
42. J. D. PASTERIS, B. WOPENKA, J. J. FREEMAN, K. ROGERS, E. VALSAMI-JONES, J. A. M. VAN DER HOUWEN and M. J. SILVA, *Biomaterials* **25/2** (2004) 229
43. W. HEIDEMANN, S. JESCHKEIT, K. RUFFIEUX, J. H. FISCHER, M. WAGNER, G. KRUGER, E. WINTERMANTEL and K. L. GERLACH, *Biomaterials* **22/17** (2001) 2371
44. J. E. BERGSMA, W.C. DE BRUIJN, F. R. ROZEMA, R. R. BOS and G. BOERING, *Biomaterials* **16/1** (1995) 25
45. C. DURUCAN and P. W. BROWN, *Adv. Eng. Mater.* **3** (2001) 227
46. A. M. GATTI and F. RIVASI, *Biomaterials* **23/11** (2002) 2381
47. K. PETERS, R. E. UNGER, C. J. KIRKPATRICK, A. M. GATTI and E. MONARI, *J. Mater. Sci. Mater. Med.* **15/4** (2004) 321
48. K. DONALDSON, P. H. BESWICK and P. S. GILMOUR, *Toxicol. Lett.* **88/1–3** (1996) 293
49. T. J. WEBSTER, C. ERGUN, R. H. DOREMUS, R. W. SIEGEL and R. BIZIOS, *Biomaterials* **22/11** (2001) 1327
50. J. E. NEVELOS, E. INGHAM, C. DOYLE, J. FISHER and A. B. NEVELOS, *Biomaterials* **20/19** (1999) 1833
51. D. GRANCHI, G. CIAPETTI, I. AMATO, S. PAGANI, E. CENNI, L. SAVARINO, S. AVNET, J. L. PERIS, A. PELLACANI, N. BALDINI and A. GIUNTI, *Biomaterials* **25/18** (2004) 4037
52. M. A. GERMAIN, A. HATTON, S. WILLIAMS, J. B. MATTHEWS, M. H. STONE, J. FISHER and E. INGHAM, *Biomaterials* **24/3** (2003) 469
53. C. H. LOHMANN, D. D. DEAN, G. KOSTER, D. CASASOLA, G. H. BUCHHORN, U. FINK, Z. SCHWARTZ and B. D. BOYAN, *Biomaterials* **23/8** (2002) :1855
54. P. H. WOOLEY and E. M. SCHWARZ, *Gene Ther.* **11/4** (2004):402